Quantum Science and Technology

PAPER • **OPEN ACCESS**

An experimental investigation of quantum frequency correlations resilience against white and colored noise

To cite this article: Linda Sansoni *et al* 2025 *Quantum Sci. Technol.* **10** 045020

IOP Publishing Quantum Sci. Technol. 10 (2025) 045020 https://doi.org/10.1088/2058-9565/adf7d0

Quantum Science and Technology

OPEN ACCESS

RECEIVED
25 March 2025

REVISED
28 July 2025

ACCEPTED FOR PUBLICATION
5 August 2025

PUBLISHED
21 August 2025

PAPER

An experimental investigation of quantum frequency correlations resilience against white and colored noise

Linda Sansoni*, Eleonora Stefanutti and Andrea Chiuri

ENEA, Nuclear Department, Via E. Fermi 45, 00100 Frascati, Italy
* Author to whom any correspondence should be addressed.

E-mail: linda.sansoni@enea.it, eleonora.stefanutti@enea.it and andrea.chiuri@enea.it

Keywords: quantum correlations, noise, quantum spectroscopy

Abstract

Quantum technologies based on photons rely on correlated pairs generated through nonlinear optics. Hence, understanding the impact of disturbances is of paramount importance for the development of this innovative field. Here we focus on the quantum spectroscopy as one of the most promising quantum technique showing a realistic perspective for a future employment. In this field, the most interesting disturbance is represented by the frequency noise. We present an experiment aimed at testing and characterizing the resilience against different levels of white and colored noise and we include simulations to generalize our findings. With this work we demonstrate that the spectroscopical properties of both the target and the noise, as well as the strength of the quantum correlations, play a crucial role and could have e huge impact on the performances, especially in terms of achievable spectral resolution. Remarkably, the presence of a specific region where the technology is always robust against any kind of noise represents an advantage allowing to deal with optimal measurements and fully exploit the capabilities of this technology.

1. Introduction

Studying the propagation of quantum light in turbulent and noisy media is crucial for advancing our understanding of fundamental physics and improving technological applications. Disturbances can significantly affect the coherence, direction, and intensity of light, posing challenges in quantum science and its applications [1]. Understanding how quantum correlations interact with such media can lead to breakthroughs in quantum communication, computation and sensing, where precision and reliability are paramount [2–4]. Indeed, this research provides valuable insights into the fundamental principles of quantum mechanics and plays a central role in the advancement of new quantum technologies that can harness quantum advantage, even in highly unpredictable conditions.

The main fields potentially affected by this detrimental aspect include imaging [5], microscopy [6] and spectroscopy [7], where the disturbance-induced fluctuations, due to absorption, scattering, and variations in the refractive index could result in a loss of the quality of the expected outcomes. In recent years, there has been growing interest in understanding and mitigating the impact of disturbances on quantum technologies operating in real-world free-space channels, often affected by turbulence and noise. Nevertheless, most of the efforts have been focused on experimental and theoretical studies regarding quantum imaging and correlation-based imaging [8, 9]. These techniques have proven effective in overcoming challenges associated with traditionally difficult free-space channels, e.g. ghost imaging (GI) in turbulent channels [10–14], quantum illumination in noisy environments [15] or chaotic-light correlation imaging against turbulence [16]. Several methods related to the *denoising* of quantum images have also been developed and tested via imaging distillation [17], image compression and reconstruction [8] or heralding of correlated photon pairs [9, 18].

However, the same attention has not been devoted to ghost spectroscopy (GS) and, more in general, to the frequency domain, as only a few examples are reported in the literature, all of which are based on environmental noise artificially introduced into the experimental setup [19].

In this study, we aim at assessing the resilience of quantum correlations under different levels of disturbance. In particular, we consider white and colored noise. White noise arises from quantum fluctuations in the field that are evenly distributed across frequencies, such as in a vacuum state or classical thermal noise in detectors. In contrast, colored noise exhibits frequency-dependent variations, typically induced by environmental coupling or quantum interactions with a thermal bath. We depict a novel approach to experimentally engineer spectral disturbance characterized by specific features, corresponding to either white or colored noise. Specifically, our investigation is built upon the framework of quantum GS (QGS) [20], initially introduced as the counter-part in the frequency domain of the quantum GI [21], as a relevant testbed to prove the effects of different kinds of noise on quantum correlations encoded in the frequency domain.

The GS has been theoretically and experimentally studied with classical (thermal) light [7] and quantum sources of photon pairs based on spontaneous parametric down conversion (SPDC) [20, 22] and spontaneous four-wave mixing [19]. Significant research efforts have also focused on comparing these two approaches, highlighting the differences and similarities between quantum and classical light sources [23–26]. The possibilities offered by the quantum regime have been deeply explored developing highly non-degenerate SPDC sources to link the mid-infrared and visible / near-infrared (NIR) range [27–31]. The frequency correlations characterizing these photon pairs have allowed to prove the feasibility of nonlinear microscopy [29, 32–34], quantum spectroscopy [30, 35–38] and quantum holography [39].

Our work represents the first analysis of the effects of colored noise on quantum frequency-correlations, as well as the first experimental realization of fully controlled white and colored noise encoded in the frequency domain to assess the performances of QGS in a highly non-degenerate configuration. We demonstrate that the QGS and the quantum correlations are resilient against white noise, while colored noise introduces a significant impact on the system. Our results reveal that colored noise is a key limiting factor in QGS resolution, with its influence amplified by stronger correlations or finer spectral targets. These findings provide experimental evidence that frequency correlations can be made robust against noisy backgrounds in free-space channels by suitably engineering and adapting the photon-pair source. Additionally, the reduction of colored noise, arising from accidental coincidence counts between uncorrelated photons, enables operations at higher brightness, which in turn allows for video-rate acquisition and more realistic integration times [40–43].

The article is organized as follows. In section 2, we describe the approach adopted to simulate white and colored noise in QGS, we then present our experimental setup in section 3 and the results in section 4. In section 5, we discuss our findings and comment on the resilience of quantum frequency correlations against noise. Finally, in the conclusive section, we provide perspectives on potential generalizations and future extensions of the present work.

2. Methods

We use the QGS as a platform to test the effects of noise on quantum correlations. QGS is based on the frequency correlations of two-photon pairs generated through SPDC in a non-linear crystal (NLC) [44]. A conceptual scheme of our analysis is shown in figure 1: here one photon from a down-converted pair in a NLC is sent on a target before being revealed by a bucket detector, the other one is analyzed in the spectral degree of freedom, and coincidences between these two photons are collected. Both channels are affected by either white or colored noise. Since SPDC through a NLC is the underlying process of our experiment, we consider the following interaction Hamiltonian [45]:

$$\mathcal{H}_{\rm int} = i\hbar\chi E_{\rm P}\left[\hat{a}_s^\dagger \hat{a}_i^\dagger + \hat{a}_s\hat{a}_i\right], \tag{1}$$

where $\hat{a}_j^\dagger$ ($\hat{a}_j$) for $j = s, i$ is the creation (annihilation) operator for photons in the signal and idler modes, respectively, χ is related to the nonlinearity of the crystal and $E_{\rm p}$ is the amplitude of the pump electric field. The corresponding evolution operator is then:

$$U = \mathrm{e}^{-\frac{i\mathcal{H}t}{\hbar}} = \exp\left[\Gamma\left(\hat{a}_s^\dagger \hat{a}_i^\dagger + \hat{a}_s\hat{a}_i\right)\right] \tag{2}$$

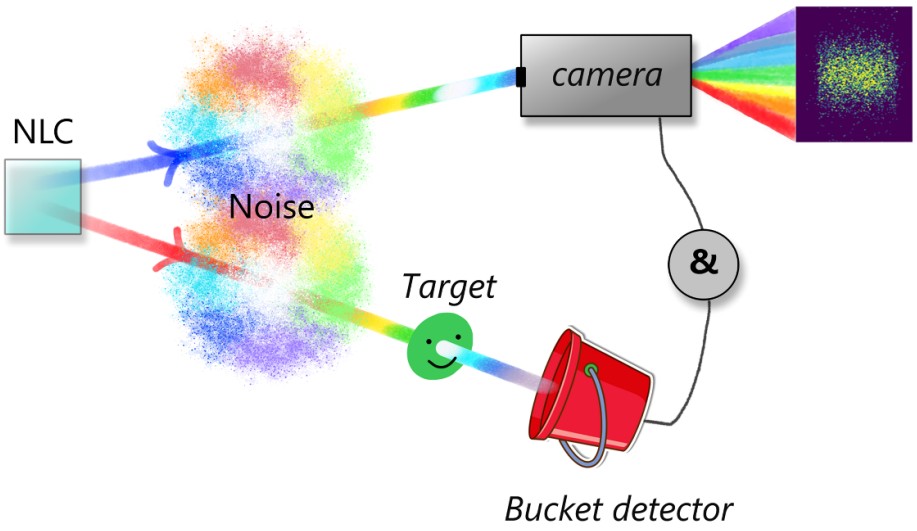

Figure 1. Conceptual scheme of the experiment: photon pairs from a non-linear crystal (NLC) disturbed by either white and colored noise are used to perform a QGS experiment [20].

where Γ is the non-linear gain. By using a Taylor expansion of the second order and considering a disentangling theorem [46], the operator in equation (2) applied to the vacuum state can be rewritten as:

$$\begin{aligned} |\Psi\rangle = U|0_s,0_i\rangle &= \frac{1}{C}\left[1+\Gamma\,\hat{a}_s^\dagger\hat{a}_i^\dagger+\frac{\Gamma^2}{2!}\left(\hat{a}_s^\dagger\hat{a}_i^\dagger\right)^2\right]|0_s,0_i\rangle \\ &= \frac{1}{C}\left[|0_s,0_i\rangle+\Gamma\,|1_s,1_i\rangle+\frac{\Gamma^2}{2!}|2_s,2_i\rangle\right] \end{aligned} \tag{3}$$

where C is a suitable normalization constant. The last expression clearly shows that the SPDC process generates either one or two photon pairs in the signal and idler modes. These modes can be defined by various degrees of freedom: spatial mode, polarization, frequency, etc. In our case, we deal with a source of frequency-entangled pairs, meaning that our signal and idler modes correspond to two distinct frequencies. Nevertheless, we have now to take into account that signal and idler photons have a spectral distribution, thus the non-vacuum part of the state generated by the SPDC, up to a normalization constant, is rewritten as

$$\begin{aligned} |\Psi\rangle = \Gamma&\int \mathrm{d}\omega_s\mathrm{d}\omega_i f(\omega_s,\omega_i)\,\hat{a}_{\omega_s}^\dagger\hat{a}_{\omega_i}^\dagger|0_s,0_i\rangle \\ &+\frac{\Gamma^2}{2!}\int \mathrm{d}\omega_s\mathrm{d}\omega_i\mathrm{d}\omega_s'\mathrm{d}\omega_i' f(\omega_s,\omega_i)f(\omega_s',\omega_i')\,\hat{a}_{\omega_s}^\dagger\hat{a}_{\omega_i}^\dagger\hat{a}_{\omega_s'}^\dagger\hat{a}_{\omega_i'}^\dagger|0_s,0_i\rangle \end{aligned} \tag{4}$$

Here $f(\omega_s,\omega_i)$ is the joint spectral amplitude (JSA) of the generated photon pairs at different frequencies ω, which contains information about the frequency distribution of the pair. While the first term of equation (4) describes the generation of a frequency correlated pair, the second term contains the product of two independent JSAs, corresponding to the generation of two independent pairs of photons. When measuring only coincidences between two photons, as in the case of the experiment depicted in figure 1, the second term in equation (4) gives rise to the detection of uncorrelated two-photon events, corresponding to those events where the two detected photons belong to different pairs [19, 47]. Since the JSA function of photon pairs is the same, this second contribution has the same spectral distribution as the correlated events described by the first term in (4), thus it can be considered as colored noise. Indeed this effect introduces a disturbance in the frequency domain: noisy photons from two different emitted pairs affect the process by introducing uncorrelated events, whose frequencies overlap with the correlated ones. The probability of generating more than one pair is proportional to the non-linear gain Γ^2 and increases with the power of the pump laser (given by $|E_\mathrm{p}|^2$). This contribution is detrimental to any process based on correlations. In particular, when exploiting frequency entanglement of SPDC pairs, the introduction of uncorrelated pairs lowers the degree of correlation between the generated photons, leading to worst performances of any protocol relying on such correlations. Moreover, when the pump laser is pulsed, this effect is further influenced by events due to coincidences between photons generated at two different times, corresponding to two consecutive pulses of the pump laser.

Noise can be minimized by adjusting experimental parameters. In particular, colored noise in SPDC due to double-pair generation can be minimized by operating in a low-rate generation regime; however this results in low count rates and, in turn, long measurement times. Assuming time-consuming measurements can still be acceptable, working at very low pump powers can completely avoid colored noise. Nevertheless, the process remains not completely noise-free. Indeed, the decreasing of the generation rate introduces other background noises, in particular spurious counts from the detection devices. This last effect is related to the main parameters commonly used to characterize the performance of a detection system:

- Dark count rate (for single-photon avalanche diode SPAD) or dark current (in the CCD camera) and electron background illumination (of the intensifier): represent signal detection when the sensor is in the dark, primarily due to thermal generation of free carriers, and it determines the minimum incident photon rate that can be detected. This parameter is relevant when the detected signals are close to these thresholds.
- Afterpulsing probability: during detection, some carriers could trigger a detection cycle not initiated by photon absorption. These non-photon-triggered pulses are referred to as afterpulsing.
- Dead time: it refers to the period after each detection event during which the detector is unable to record another event. Setting short dead times allows for higher count rates, however it may also increase afterpulsing events, as well as dark counts.

The spurious contributions due to the aforementioned phenomena can be modeled as white noise. White noise is generally harder to reduce through correlation techniques [48–51], but it can often be mitigated by averaging over large datasets or using filters designed to reduce specific types of noise.

A figure of merit often used to evaluate the noise contribution of a setup is the signal-to-noise ratio, which, in our case, is given by the coincidence-to-accidental ratio (CAR) [52–54]. It can be calculated as:

$$\mathrm{CAR} = \frac{N_{\mathrm{cc}}}{N_{\mathrm{acc}}}, \tag{5}$$

where N_{cc} is the raw two-photon coincidence counts, while N_{acc} denotes the accidental coincidence counts (uncorrelated photon pairs). Usually, experiments based on correlations are performed with a CAR value as high as possible. At low pump power, the CAR results to be limited by dark counts and environmental noise (white noise). Conversely, at higher pump powers, the CAR is limited by after-pulsing and multi-pair generation (colored noise), which increase the probability of accidental coincidence counts between signal and idler photons belonging to different pairs.

Depending on the process under consideration and the maximum acceptable noise, the parameters of an experiment are typically defined according to CAR value. However, by investigating the effects of white and colored noise in the frequency degree of freedom of a QGS experiment, we demonstrate that the CAR alone is not a sufficient figure of merit to assess whether the protocol is noise-resilient. A crucial factor is the knowledge about the nature of the disturbance. Indeed, we observe that for low values of the CAR the QGS is resilient against white noise, while it is vulnerable against colored noise. It is important to note that the amount of white and colored noise depends on the setup equipment and its parameters. Therefore, a comprehensive characterization can be carried out before the experiment in order to find the optimal settings. In our case, prior knowledge allowed us to fix some parameters at their optimal value—such as detector dead time, source brightness, coincidence time-window- while varying others that we found most relevant to our investigation, as pump power density, spectral bandwidth of the target, strength of frequency correlations.

3. Experiment

Our strategy relies on the nonlinear process of SPDC, wherein a small fraction of photons from a pump laser is converted into correlated photon pairs with lower energies. We consider a non-degenerate configuration, where the signal and idler down-converted photons are in the NIR and visible spectral range, respectively. The QGS approach exploits the intrinsic frequency correlations between the generated signal and idler photons to enable spectral characterization of infrared photons by performing measurements on their visible counterparts [20].

Figure 2 illustrates a schematic of our QGS experimental setup. The excitation beam was generated by a pulsed laser operating at a repetition rate of 40 MHz with a pulse duration of 8 ps; the pump spectrum was centered at $\lambda_{\mathrm{P}} = 532$ nm, with a spectral bandwidth of 0.23 nm. The laser beam was used to illuminate a 2 mm-long periodically poled potassium titanyl phosphate (ppKTP) crystal (manufactured by SLF Svenska Laserfabriken AB), with a poling period of 9.725 μm. The type-0 down-conversion process generated pairs of collinear photons with vertical polarization, matching that of the pump laser. The phase matching condition

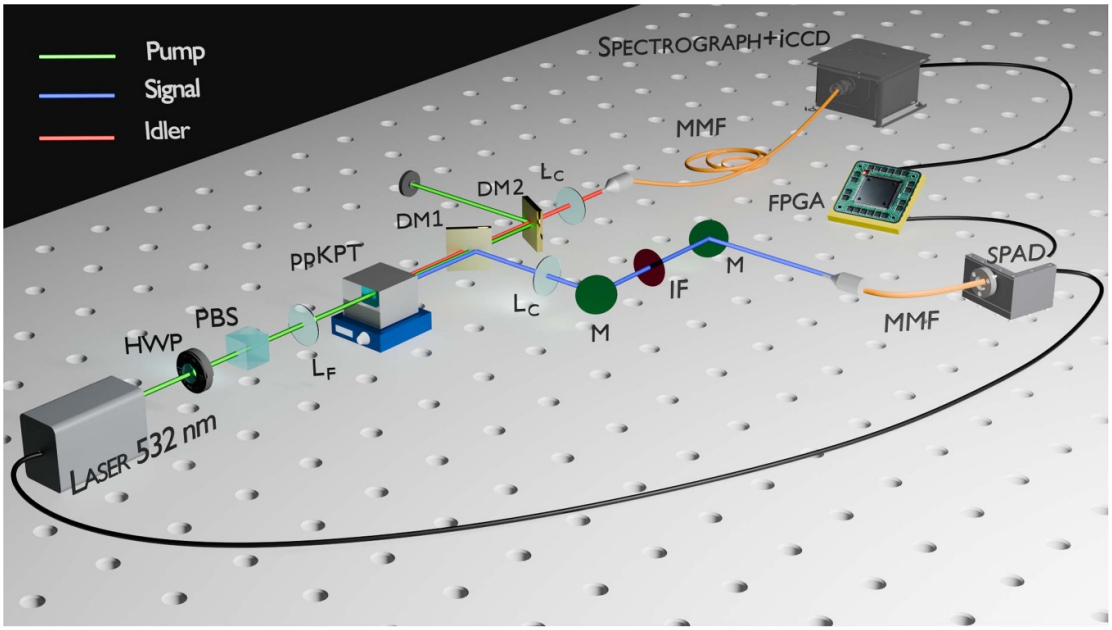

Figure 2. Experimental setup for QGS measurements. The optical elements in figure are HWP: half-wave plate, PBS: polarizing beam splitter, ppKTP: poled potassium titanyl phosphate non-linear crystal, DM1: dichroic mirror for separating signal (reflected arm) and idler (transmitted arm) photons, DM2: dichroic mirror used to remove the pump beam from the idler path, IF: interference filter, L_F: focusing lens ($f = 250$ mm), L_C: collimating lens, M: mirror, MMF: multi-mode fiber.

was optimized with the crystal temperature, which could be tuned using a customized thermoelectric heating cell and a temperature controller with a precision of 0.1 °C. The operating temperature was kept at $T = 30\,^{\circ}\mathrm{C}$, at which the signal photons are emitted at a central wavelength $\lambda_i \approx 1550$ nm, corresponding to an idler wavelength $\lambda_s \approx 810$ nm. The idler and signal photons were separated using a DM1. The signal photon on the reflected arm of DM1 was directed to an interference filter (IF) centered at 1550 nm with a bandwidth of 10 nm and then coupled to a SPAD (MPD PDM-IR), acting as a bucket detector. The SPAD was triggered by the sync-out TTL (transistor-transistor logic) signal coming from the laser. In order to perform frequency-resolved measurements, the idler photon on the transmitted arm of DM1 was sent to a spectrograph (Andor Kymera 328I-A-SIL) equipped with a diffraction grating (600 lines/mm) and an intensified CCD (Andor iSTAR iCCD DH334T-18U-73). Both idler and signal photons were collimated and subsequently collected through MMFs. The pump laser was removed by a second DM2 along the idler path.

To measure signal-idler photon coincidences, the acquisition from the camera was synchronized with the SPAD, taking into account optical path length differences between signal and idler photons, the bucket detector response time, and the other electronic delays. Thus the correct delay on the idler was introduced using a multi-mode optical fiber of appropriate length and finely adjusted with a field programmable gate array (FPGA) board connected to the SPAD detector. The raw data acquired from our measurements represent the photon counts recorded by the iCCD for each pixel in photon-counting mode. Since the horizontal coordinate of each pixel corresponds to a wavelength, we obtained a spectral analysis of the idler photons detected in coincidence with the signal counterpart recorded by the bucket detector. As the spatial distribution of the collected idler photons was not of interest, an integration over the vertical coordinate (vertical binning) was performed to obtain the total photon counts along with their spectral distribution. All final spectra were smoothed using a Savitzky–Golay filter. Given the idler spectrum, the corresponding signal spectral distribution was inferred as a consequence of the phase-matching condition ($\lambda_s = (1/\lambda_\mathrm{P} - 1/\lambda_i)^{-1}$).

By properly adjusting the delay between iCCD and SPAD, we collected photon counts corresponding to signal-idler coincidences and accidental coincidence counts due to uncorrelated photons. This allowed us to perform the ghost measurements of the IF and estimate the CAR of our source as a function of the pump power. The average power of our laser was tunable up to 200 mW, and the CAR dependence on pump power was characterized over the entire range. To obtain lower CAR values we have inserted a lens before the crystal to focus our pump beam and evaluated the CAR as a function of the pump power normalized to the beam area, i.e. pump power density. The integration time was optimized for each measurement to ensure statistically significant photon counts across varying the pump power. As a reference, we measured the spectral properties of the source with the 2 mm ppKTP NLC removing the IF from the signal path, setting the pump power at an optimal CAR value.

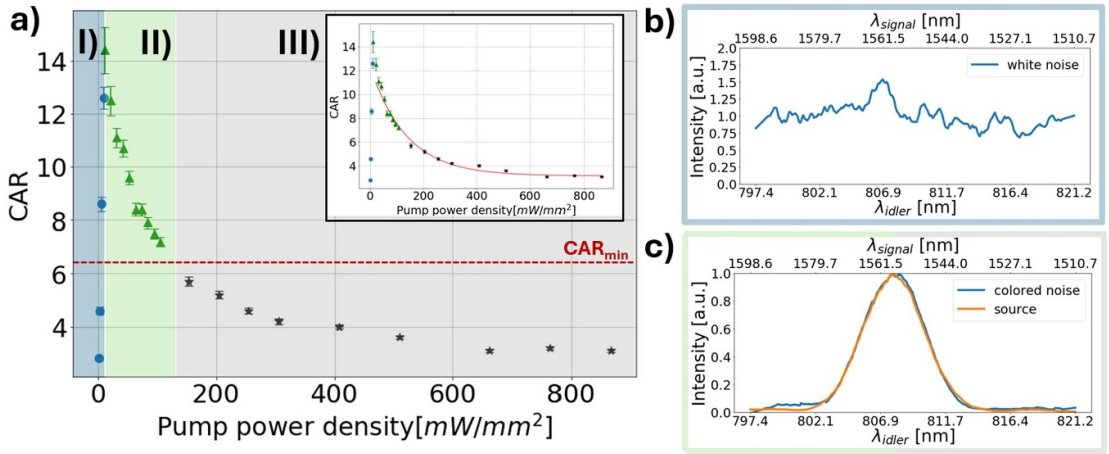

Figure 3. (a) CAR as a function of the pump power density. At low values of pump power density (region I, blue shaded with blue circles) white noise is dominant, for values of CAR above CAR_{min} (red dashed line) in region II (green shaded with green triangles) noise is negligible, for values below CAR_{min} in region III (gray shaded with black stars) the contribution to noise is mainly due to colored noise. (b) and (c) spectra for white (b) and colored (c) noise corresponding to regions I and III of panel a. The error bars have been calculated propagating the Poissonian fluctuations on the photon counts.

4. Results

In figure 3 we present an analysis of the noise in relation to the CAR of our system. Panel (a) displays the measured CAR as a function of the pump power density.

The data show a steep rise, followed by a peak and a slow decrease. The decreasing trend (panel (a), top right inset) has been fitted with a negative exponential function of the type $CAR(P) = Ae^{-\frac{P}{P_o}}$, where A is the maximum CAR and P_o denotes the pump power density at which the CAR is lowered by a factor e. Using the fitting parameters, the CAR corresponding to $P = P_o$ has a value of $CAR_{min} = (6.5 \pm 0.1)$, that can be interpreted as the minimum CAR threshold above which the impact of colored noise on the experiment becomes negligible (figure 3(a) green triangles). Although the CAR_{min} value depends on the specific equipment adopted for the setup, its limit is indirectly taken into account in various experiments, where the parameters are adjusted to remain far enough from this threshold to ensure successful experiments [55]. As a matter of fact, for CAR values below CAR_{min}, colored noise becomes dominant. Depending on the pump power density, we can identify other two regions: the first one where the noise is due to white events, such as dark counts, is marked in panel (a) as region I (blue shaded with blue circles). Measured noise as a function of the signal and idler wavelengths corresponding to this region is shown in figure 3(b), where a flat spectrum with random fluctuations is observed. At higher pump power densities, in region III of panel (a) (gray shaded with black stars) the noise is introduced by colored events, whose spectral distribution is shown in figure 3(c). Here, both the source spectrum (orange curve) and the noise spectrum (blue curve) are shown. The two distributions are clearly the same, meaning that the noise presents spectral features that overlap with the process under investigation. As a result, the noise introduces disturbances that may be detrimental, as we will demonstrate later. Obviously, when setting up an experiment, the optimal working-point corresponds to a CAR as high as possible, i.e. on the peak of figure 3(a). However, selecting a pump power density within the range corresponding to region II in panel (a) can still be advantageous, depending on other factors such as signal rates and measurement times.

After characterizing the CAR and noise spectrum, we performed a QGS experiment with the aim of reconstructing the spectral image of an IF (full width at half maximum, FWHM = 10 nm) at different CAR values, corresponding to the three different regions of figure 3: one at low CAR dominated by white noise (panel I), one at the optimal CAR (panel II) and the last at low CAR dominated by colored noise (panel III). The results are shown in figure 4 panels (I), (II) and (III), respectively.

5. Discussion

Our results characterize the effect of white and colored noise on quantum correlations, in particular we observe that colored noise lowers the resolution of the QGS. This is very clear from figure 4 III: as the pump power density increases, we observe a broadening of the ghost spectrum (orange curve) compared to the optimal spectrum (blue line corresponding to a $P = 31.58\ mW/mm^2$ and a CAR$\approx$ 11), which tends to the

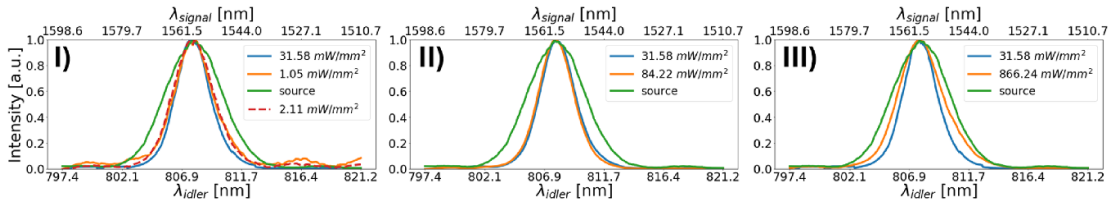

Figure 4. Comparison between the experimental spectra of the source (green curve), the IF ghost at different CAR values (orange and red curves) corresponding to figure 3(a) and a ghost spectrum at optimal CAR (blue curve corresponding to $P = 31.58\ mW/mm^2$). (I) QGS spectra in presence of white noise corresponding to low pump power densities. (II) QGS spectrum at optimal CAR. Here quantum correlations are preserved and the QGS measurements are fast and reliable. (III) Ghost spectra in presence of colored noise: the presence of colored noise dilutes quantum correlations and broadening of the spectrum is observed.

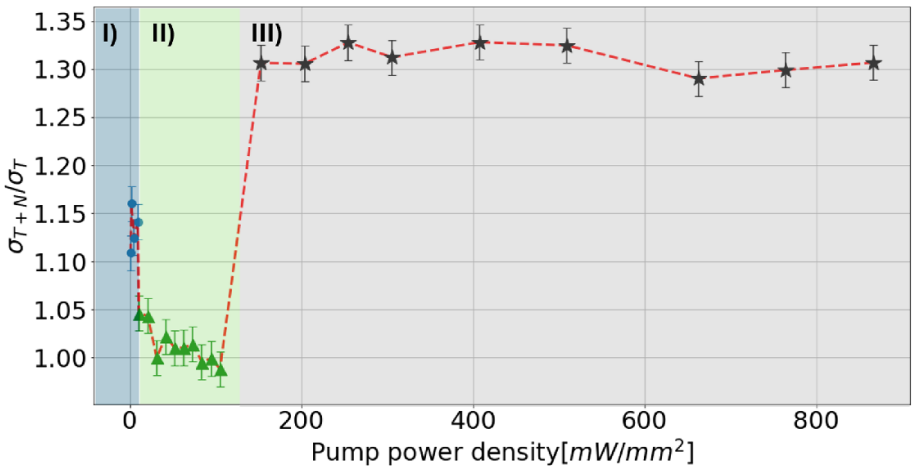

Figure 5. Experimental ghost width (σ_{T+N}) normalized to the optimal one (σ_T) as a function of the pump power density. Regions I to III correspond to the same regions of figure 3(a). The region II with green triangles corresponds to optimal experimental setting where we do not observe any broadening. In region III (black stars), colored noise strongly affects the QGS spectrum with a 30% increase of the ghost width. In region I a slight broadening is observed mainly due to a residue of colored noise.

width and shape of the source spectral distribution (green curve). In this condition the QGS protocol is no longer reliable, as its resolution is heavily reduced: here quantum correlations are strongly affected by colored noise and the quantum protocol fails. The optimal parameters—for CAR above CAR_{min}—lead to an optimal QGS protocol, whose results are shown in figure 4(II): the ghost spectrum of the target IF is retrieved without broadening (curves blue and orange) and with high signal rates.

In figure 4(I) we compare the ghost spectrum of the target IF taken at low pump power densities with the source spectrum (green line) and the ghost at optimal CAR (blue curve). For these values of pump power density the CAR is low and the noise relevant, but it is mainly due to white events. At the cost of long measurement times, we expected to reconstruct the ghost spectrum without alterations, meaning that the QGS (and thus quantum correlations) is robust against white noise. However we observe a slight broadening. To further investigate this result we have reported the measured broadening as a function of the pump power density. The data is shown in figure 5 where we plot as a measure of the broadening, the experimental width of the ghost spectrum (σ_{T+N}) normalized to the optimal one (σ_T) for various pump power densities, corresponding to the regions highlighted in figure 3(a). Here we can observe, as expected, that no broadening is present for optimal CAR values (region II, green shaded with green triangles), while a drastic increase in the spectral width is evident for high pump power densities (region (III), gray shaded with black stars). The slight broadening observed in figure 4(I) is evident also in region (I) of figure 5 (blue shaded with blue dots). Here the broadening is less than for high pump power densities, but still visible. We can trace back this behavior to a residue of colored noise, which is overlapped with the white background, as indicated by the small central peak visible in figure 3(b).

To ascertain that the broadening is due to the presence of colored noise, we have compared the experimental ghost of figure 4(III) (blue spectrum), corresponding to a noise of 30%, with a theoretical model (orange dashed line). The results are shown in figure 6: the two shapes overlap, showing that the loss of resolution can be ascribed to the presence of colored noise. For a more general perspective, we have

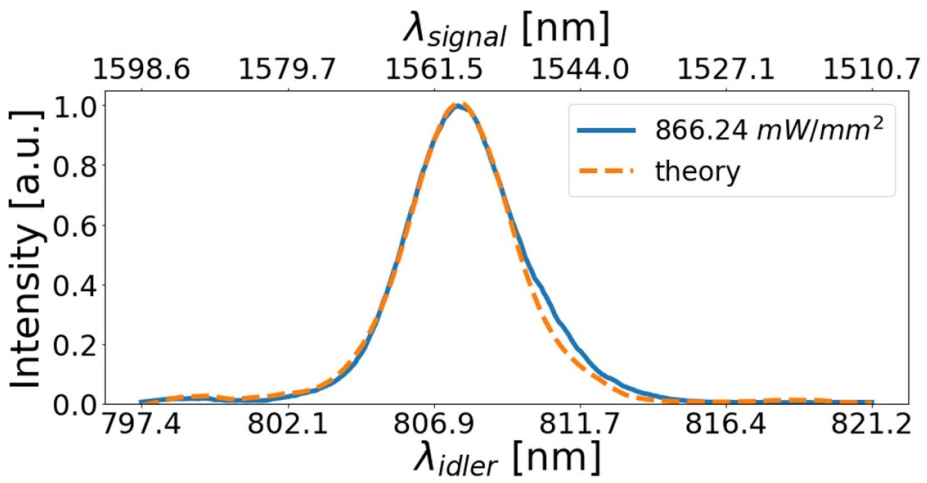

Figure 6. Comparison between experimental quantum ghost spectrum in presence of 30% colored noise (blue curve) and the theoretical simulation (orange dashed line).

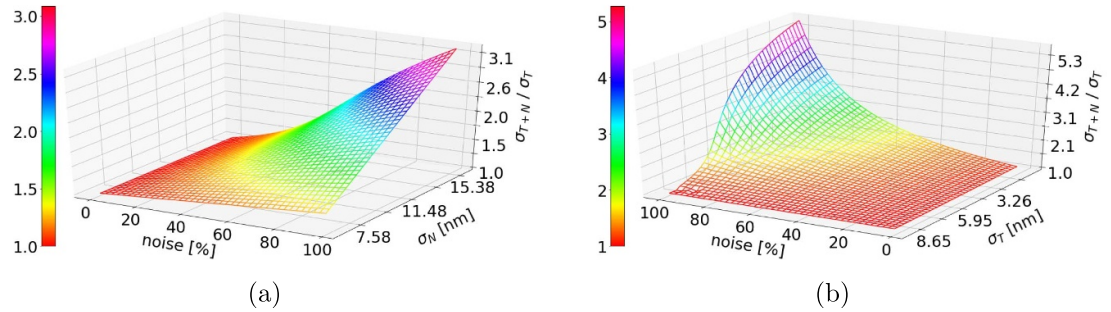

Figure 7. Width of the spectrum resulting from the QGS analysis of a target filter normalized to the ideal spectral width (σ_{T+N}/σ_T) as a function of the amount of colored noise introduced and (a) the width of the noise spectrum σ_N of the IR photon or (b) the width of the IR target.

investigated how the resolution of the QGS in presence of colored noise is affected by other parameters such as the strength of the frequency correlations and the spectral width of the analyzed target.

To this extent, we considered a QGS protocol on a target of fixed spectral width (FWHM of 10 nm in the IR, as in the experiment) and varied the amount of noise and the strength of the quantum correlations. This last parameter is linked to the width of the SPDC source, indeed the more correlated the JSA, the broader the spectra of signal and idler.

We have thus simulated the bandwidth of the QGS spectrum normalized to the ideal target bandwidth as a function of the amount of noise and the bandwidth of the colored noise. The simulation is shown in figure 7(a). Here we can observe that the effect of colored noise is drastic for strongly correlated pairs, indeed the broader the noise bandwidths ($_{\sigma_N}$ in the figure) the larger the width of the QGS. On the other hand weak correlations are more resilient to the introduction of noise, as a large percentage of noise is needed to increase the QGS bandwidth. We have then analyzed the behavior of the QGS broadening in presence of noise with a fixed correlation strength of the source and varying the spectral width of the target. The results are shown in figure 7(b). In this case the narrower the target, the stronger the effect of colored noise on QGS broadening.

For a better understanding of the dramatic effect of colored noise on the resolution of a QGS, we performed a simulation of the resolving power of two peaks (FWHM = 10 nm @1550 nm corresponding to FWHM = 2.8 nm @810 nm) by varying their spectral distance and the amount of colored noise (with fixed bandwidth). We modeled the two peaks as Gaussian shapes and the resolving power as

$$R_P = \frac{x_0^1 - x_0^2}{\sigma_1 + \sigma_2} \tag{6}$$

where $x_0^{1(2)}$ is the central wavelength of the first (second) peak and $\sigma_{1(2)}$ are their respective standard deviations, or half widths. The two peaks can be resolved as long as $R_P > 1$. In figure 8 we show the behavior of R_P as a function of the distance between the central wavelengths—varying between 0.5 and 3 nm for the

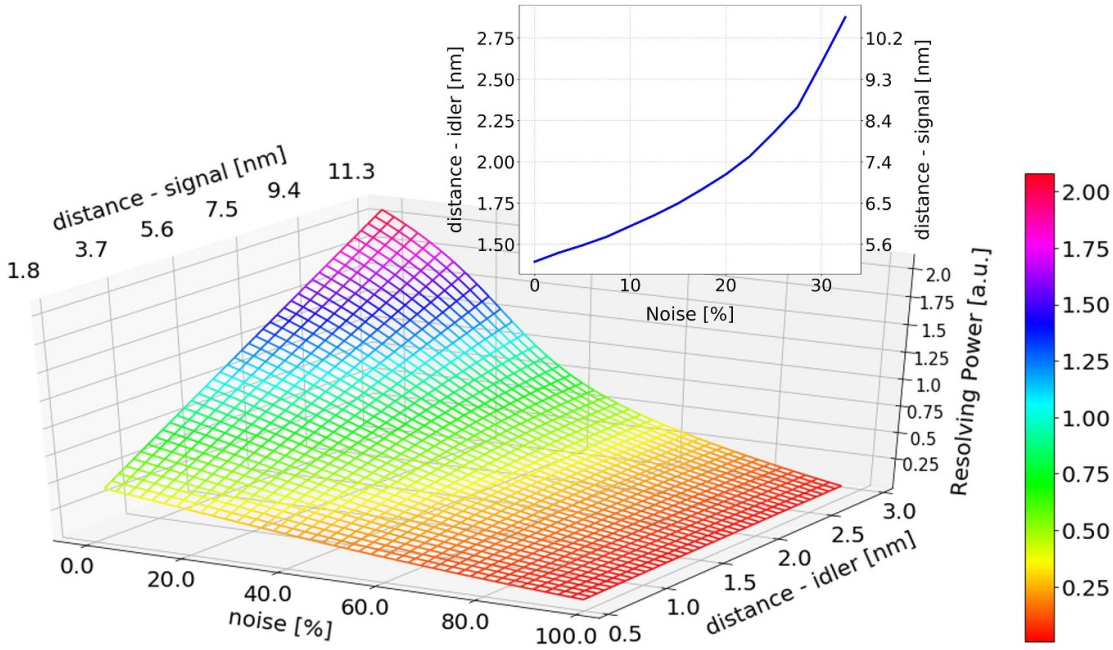

Figure 8. Resolving power R_P as a function of the distance between the central wavelengths and the amount of colored noise. Here we have considered a spectrum composed by two peaks equal to the one obtained with power density $= 31.58\ mW/mm^2$. In this system we have introduced different percentages of colored noise repeating the simulation for different peak separations. Each resulting noisy spectrum was fitted using two Gaussian curves of the form $d + a \cdot \exp(-(x - x_0)^2/(2 \cdot \sigma^2))$. R_P has been calculated by using the parameters obtained from these Gaussian fits, where, $R_P > 1$ (< 1) means the two peaks can (cannot) be separated. In the inset is reported a cut of the main graph for $R_P = 1$. Here it is visible how for short distances between the two peaks, just a very low amount of noise is acceptable.

idler and between 1.8 and 11.3 nm for the signal—and the amount of colored noise (with the same spectral distribution of the source, which is much larger than the combined spectral distribution of the two peaks). We can clearly observe that the resolving power dramatically decreases as soon as noise increases and, as expected, this effect becomes more pronounced when the peak separation is smaller. Nonetheless, even for two peaks that are 3 nm apart, an amount of noise around 25%–30% is sufficient to prevent their resolution. This is well visible in the inset where we show a cut for $R_P = 1$ and plot the amount of maximum acceptable noise as a function of the distance between the two peaks. As expected, the closer the two peaks, the less the amount of acceptable noise.

6. Conclusions

In this manuscript, we have provided an experimental investigation regarding the implementation of white and colored noise and their effect on quantum correlations. We have shown that the CAR value is not sufficient to determine the effect of noise on quantum correlations, as the nature of the noise itself plays a crucial role: decoherence becomes relevant in the presence of colored noise, while quantum correlations are more robust against white noise. Our study is grounded in a platform that is attracting a broad interest for its possible applications and promising perspectives towards the 3D and remote sensing, i.e. the QGS. Technologies based on the *ghost* approach rely on the use of two types of correlations: semiclassical, i.e. where a source of thermal or pseudo-thermal light is employed, or quantum. Since the latter has shown better performances [23, 25], we have explored this field. We have found that colored noise plays a critical role in degrading the achievable spectral resolution of QGS. This effect becomes increasingly significant when the frequency correlations are stronger or when the spectral features to be retrieved are particularly narrow. Recent experimental advances have pushed the capabilities of correlation-based technologies far beyond the expected boundaries thanks to their demonstrated advantages related to the visibility, the contrast-to-noise ratio and the resolution. Their performances can be extended and improved employing also higher-order correlations between more particles, as demonstrated with quantum and classical correlations [56, 57]. These promising perspectives towards a realistic employment underscore the necessity of the systematic study presented in this work, which aims at a better understanding on how to proceed on the road to reliable quantum technologies.

Data availability statement

The data cannot be made publicly available upon publication because no suitable repository exists for hosting data in this field of study. The data that support the findings of this study are available upon reasonable request from the authors.

Acknowledgment

The Authors thank Max Widarsson and Patrick Mutter from SLF Svenska Laserfabriken for providing the source crystal, Federico Angelini for the fruitful discussions, and Marcello Nuvoli for the fabrication of mechanical holders.

Conflict of interest

The authors declare that they have no competing interests.

Funding

This project is funded within the QuantERA II Programme (Qucaboose Project), that has received funding from the EU H2020 research and innovation programme under GA No 101 017 733, and with funding organization NQSTI (Italy).

Authors' contribution

Conceptualization, Methodology, Experiment, Formal Analysis and Visualization, Writing, Review, and Editing: All Authors; Funding acquisition: A C.

ORCID iDs

Linda Sansoni 0000-0002-4445-1036
Eleonora Stefanutti 0000-0002-2833-7049
Andrea Chiuri 0000-0001-9733-0740

References

[1] Clerk A A, Devoret M H, Girvin S M, Marquardt F and Schoelkopf R J 2010 *Rev. Mod. Phys.* **82** 1155–208
[2] Karpiński M, Davis A O C, Sośnicki F, Thiel V and Smith B J 2021 *Adv. Quantum Technol.* **4** 2000150
[3] Lib O and Bromberg Y 2022 *Nat. Phys.* **18** 986–93
[4] Mukamel S *et al* 2020 *J. Phys. B: At. Mol. Opt. Phys.* **53** 072002
[5] Padgett M J and Boyd R W 2017 *Phil. Trans. R. Soc. A* **375** 20160233
[6] Bowen W P, Chrzanowski H M, Oron D, Ramelow S, Tabakaev D, Terrasson A and Thew R 2023 *Contemp. Phys.* **64** 169–93
[7] Janassek P, Herdt A, Blumenstein S and Elsäßer W 2018 *Appl. Sci.* **8** 1896
[8] Morris P A, Aspden R S, Bell J E C, Boyd R W and Padgett M J 2015 *Nat. Commun.* **6** 5913
[9] Johnson S, McMillan A, Torre C, Frick S, Rarity J and Padgett M 2022 *Opt. Continuum* **1** 826
[10] Hardy N D and Shapiro J H 2011 *Phys. Rev. A* **84** 063824
[11] Dixon P B *et al* 2011 *Phys. Rev. A* **83** 051803
[12] Shi D, Fan C, Zhang P, Zhang J, Shen H, Qiao C and Wang Y 2012 *Opt. Express* **20** 27992–8
[13] Freitas B A, Zhang Y, England D G, Lundeen J S and Sussman B J 2025 *Opt. Quantum* **3** 78–83
[14] Li C, Wang T, Pu J, Zhu W and Rao R 2010 *Appl. Phys. B* **99** 599–604
[15] Gregory T, Moreau P A, Toninelli E and Padgett M J 2020 *Sci. Adv.* **6** eaay2652
[16] Scala G, Massaro G, Borreggine G, Lupo C, D'Angelo M and Pepe F V 2024 *Eur. Phys. J. Plus* **139** 1010
[17] Fuenzalida J, Basset M G, Töpfer S, Torres J P and Gräfe M 2023 *Sci. Adv.* **9** eadg9573
[18] Pearce E, Phillips C C, Oulton R F and Clark A S 2020 *Appl. Phys. Lett.* **117** 054002
[19] Sanna M, Rizzotti D, Signorini S and Pavesi L 2024 *Adv. Quantum Technol.* **7** 2300159
[20] Chiuri A, Angelini F, Santoro S, Barbieri M and Gianani I 2023 *ACS Photonics* **10** 4299–304
[21] Pittman T B, Shih Y H, Strekalov D V and Sergienko A V 1995 *Phys. Rev. A* **52** R3429–32
[22] Chiuri A, Angelini F, Gianani I, Santoro S, Sansoni L, Stefanutti E and Barbieri M 2025 *Eur. Phys. J. Plus* **140** 186
[23] Bennink R S, Bentley S J, Boyd R W and Howell J C 2004 *Phys. Rev. Lett.* **92** 033601
[24] O'Sullivan M N, Chan K W C and Boyd R W 2010 *Phys. Rev. A* **82** 053803
[25] Chiuri A, Gianani I, Cimini V, De Dominicis L, Genoni M G and Barbieri M 2022 *Phys. Rev. A* **105** 013506
[26] Gatti A, Brambilla E, Bache M and Lugiato L A 2004 *Phys. Rev. Lett.* **93** 093602
[27] Yabushita A and Kobayashi T 2004 *Phys. Rev. A* **69** 013806
[28] Chan K W C, O'Sullivan M N and Boyd R W 2009 *Phys. Rev. A* **79** 033808
[29] Aspden R S *et al* 2015 *Optica* **2** 1049–52
[30] Tashima T, Mukai Y, Arahata M, Oda N, Hisamitsu M, Tokuda K, Okamoto R and Takeuchi S 2024 *Optica* **11** 81–87

[31] Neves S, Kartiyasa A, Ghosh S, Gaulier G, La Volpe L and Wolf J P 2024 *APL Photon.* **9** 096108
[32] Samantaray N, Ruo-Berchera I, Meda A and Genovese M 2017 *Light Sci. Appl.* **6** e17005–17005
[33] Kalashnikov D, Paterova A, Kulik S and Krivitsky Leonid A 2016 *Nat. Photon.* **10** 98–101
[34] Gili V F, Piccinini C, Safari Arabi M, Kumar P, Besaga V, Brambila E, Gräfe M, Pertsch T and Setzpfandt F 2022 *Appl. Phys. Lett.* **121** 104002
[35] Lindner C, Wolf S, Kiessling J and Kühnemann F 2020 *Opt. Express* **28** 4426–32
[36] Mukai Y, Arahata M, Tashima T, Okamoto R and Takeuchi S 2021 *Phys. Rev. Appl.* **15** 034019
[37] Kaufmann P, Chrzanowski H M, Vanselow A and Ramelow S 2022 *Opt. Express* **30** 5926–36
[38] Kurita T, Mukai Y, Okamoto R, Arahata M, Tashima T, Ota H, Tokuda K and Takeuchi S 2025 *Phys. Rev. Appl.* **23** 014061
[39] Töpfer S, Basset M G, Fuenzalida J, Steinlechner F, Torres J P and Gräfe M 2022 *Sci. Adv.* **8** eabl4301
[40] McCarthy A *et al* 2025 *Optica* **12** 168–77
[41] Fisher-Levine M and Nomerotski A 2016 *J. Instrum.* **11** C03016
[42] Nomerotski A 2019 *Nucl. Instrum. Methods Phys. Res. A* **937** 26–30
[43] Vidyapin V, Zhang Y, England D and Sussman B 2023 *Sci. Rep.* **13** 1009
[44] Boyd R W 2020 *Nonlinear Optics* (Academic)
[45] Walls D and Milburn G J 2008 *Quantum Optics* (Springer)
[46] Rossmann W 2002 (Lie Groups) *Oxford Graduate Texts in Mathematics* (London, England: Oxford University Press)
[47] Signorini S and Pavesi L 2020 *AVS Quantum Sci.* **2** 041701
[48] Paz-Silva G A, Norris L M and Viola L 2017 *Phys. Rev. A* **95** 022121
[49] Wang Y X, Bringewatt J, Seif A, Brady A J, Oh C and Gorshkov A V 2024 Exponential entanglement advantage in sensing correlated noise (arXiv:2410.05878)
[50] Ji Zou Stefano Bosco D L 2024 *npj Quantum Inf.* **10** 46
[51] Massaro G, Barile B, Scarcelli G, Pepe F V, Nicchia G P and D'Angelo M 2024 *Laser Photon. Rev.* **18** 2301155
[52] Guo K, Christensen E N, Christensen J B, Koefoed J G, Bacco D, Ding Y, Ou H and Rottwitt K 2017 *Appl. Phys. Express* **10** 062801
[53] Kumar M, Kumar P, Vega A, Weissflog M A, Pertsch T and Setzpfandt F 2021 *Appl. Phys. Lett.* **119** 244001
[54] Hojo M, Tani S, Kobayashi Y and Tanaka K 2023 *Sci. Rep.* **13** 8520
[55] Pitsch C, Walter D, Grosse S, Brockherde W, Bürsing H and Eichhorn M 2021 *Appl. Opt.* **60** F66–F70
[56] Hodgman S S, Bu W, Mann S B, Khakimov R I and Truscott A G 2019 *Phys. Rev. Lett.* **122** 233601
[57] Chan K W C, O'Sullivan M N and Boyd R W 2009 *Opt. Lett.* **34** 3343–5